

## ADSORPTION OF NEUTRAL RED DYE FROM AQUEOUS SOLUTIONS BY NATURAL ADSORBENT: AN EQUILIBRIUM, KINETIC AND THERMODYNAMIC STUDY

Ali Rıza Kul<sup>1</sup>, Eda Gökırmak Söğüt<sup>2</sup>, Necla Çalışkan Kılıç<sup>1</sup>

<sup>1</sup>Department of Physical Chemistry, Faculty of Science, Yuzuncu Yıl University, Van, 65080, TURKEY

<sup>2</sup>Van Security School, Yuzuncu Yıl University, Van, 65080, TURKEY

**ABSTRACT.** This study investigates the adsorption of neutral red (NR) on the natural clayey material of Adilcevaz/ Bitlis located the northwest of Van Lake in Eastern Anatolia (Turkey). The adsorbent used was characterized by XRD, XRF, FTIR, SEM and TG-DTA analyzes. The effect of various parameters such as pH, contact time, initial concentration and temperature on NR removal was investigated using a batch process to optimize the maximum adsorption conditions. Equilibrium data for NR adsorption were analyzed using nonlinear two-parameter isotherms such as Langmuir, Freundlich, Dubinin-Radushkevich, and Tempkin, and three-parameter isotherm models, such as nonlinear Redlich-Peterson, Sips, and Koble-Corrigan. The modelling results showed that it was best adapted to the Freundlich isotherm model for the NR dye, with relatively higher  $R^2$  values and smaller S.E. The maximum adsorption capacity obtained from the experimental data was determined to be  $4.2810 \text{ mg g}^{-1}$ . The adsorption process follows pseudo-second-order kinetics with a rate constant of  $0.0110 \text{ g mg}^{-1} \text{ min}^{-1}$ . The thermodynamic parameters indicate that a physical mechanism controls the NR adsorption on the natural clay and spontaneously occurs.

*Keywords.* Adsorption, dye, natural clay, non-linear isotherm models, thermodynamic, kinetic

 edagokirmak@yyu.edu.tr -Corresponding author; alirizakul@yyu.edu.tr; ncaliskan7@hotmail.com  
 0000-0001-9331-775X; 0000-0002-7707-3924; 0000-0001-5451-3192.

© 2021 Ankara University

Communications Faculty of Sciences University of Ankara Series B: Chemistry and Chemical Engineering

## 1. INTRODUCTION

The supply of fresh water is becoming increasingly difficult due to industrial, urban, or agricultural human activities. As water pollution reaches unavoidable levels over time, international interest in water-related studies is increasing. Dye aggregation in waste water from different industries such as textile, paper, cosmetics, printing and plastics is one of the primary sources of water pollution [1]. These are divided into three according to their nuclear structure: anionic dyes (acidic and reactive), non-ionic dyes (disperse) and cationic dyes (basic) [2].

Neutral Red (NR) is a cationic dye ( $C_{15}H_{16}N_4HCl$ ) that is often used as a pH indicator in analytical laboratories and in case of decomposition, which produces hazardous products such as carbon monoxide (CO), carbon dioxide ( $CO_2$ ), nitrogen oxides and hydrogen chloride [3]. These products threaten not only people but also animals and the natural environment. For this reason, waste containing neutral red should be removed [4]. Some methods such as ion exchange [5], chemical precipitation [6], photocatalysis [7], membrane technologies [8] and adsorption [9] are widely used in dye removal. The adsorption method is particularly desirable among these methods due to its simplicity of design, high removal efficiency, and ease of use [10]. Basically, any solid material having a porous structure can be used as an adsorbent. Some researchers have studied dye adsorption from aqueous solutions using many adsorbents such as activated carbon, clay, peat, chitin, silica and others. In particular, commercial activated carbon has been used effectively in the process of removing dye and heavy metals from aqueous phases [11]. Unfortunately, the use of commercial activated carbon is not economical due to high cost and regeneration problems. Apart from the adsorption capacity of the adsorbent, other parameters such as cost of production and regeneration, availability, environmental compatibility and energy consumption are also crucial in the choice of adsorbent [9]. For this reason, the related studies aim to find a more cost-effective and effective adsorbent when compared to activated carbon [11]. Clays have a great potential for removing contaminants such as heavy metals, wastewater dyes and organic compounds due to their interesting physicochemical properties (layer structure, high surface area and high

cation exchange capacity) [12,13]. Many studies in recent years have focused on the investigation of locally available clay as low-cost adsorbents [14]. Van lake basin is rich in some industrial raw materials. Clayey soils in the region are used by the people of the region for personal cleaning applications and for the production of an oven called “tandır” which is used for baking bread [15]. It is very important to determine the chemical, physicochemical and adsorptive properties of the materials that can be used as industrial raw material in the region and to use the raw material without pretreatment, i.e. without energy expenditure and secondary chemical waste. Adsorption and desorption of organic molecules onto clay are primarily concerned with the properties of the clay surface and the chemical properties of the molecules [13]. Cationic dye molecules have a very high affinity for clay surfaces and are easily adsorbed when treated with clay suspensions.

This study focuses on the use of a local raw material containing natural clay minerals as an adsorbent for Neutral Red (NR) adsorption from aqueous solutions. The adsorbent was characterized by X-ray fluorescence (XRF), Fourier transform infrared spectroscopy (FT-IR), X-ray diffraction (XRD), thermogravimetric and differential thermal analysis (TG-DTA) and scanning electron microscope (SEM) techniques. Batch experiments were carried out to determine the equilibrium time, and experimental data were applied to different isotherms and kinetic models to understand the adsorption process of NR on natural clay.

## 2. MATERIALS AND METHODS

### 2.1. Adsorbent

The natural clay samples collected from the Adilcevaz/Bitlis region were powdered in a mortar. No pretreatment has been applied to the material. After passing through a 350-mesh sieve, it was stored in the polymer bags. The natural pH value of the clay suspension was determined as  $\sim 8.3 \pm 0.1$  by pH meter.

## 2.2. Adsorbate

Neutral Red (NR), a cationic dye, was obtained from Fluka. The dye structure containing a secondary amine group is presented in Figure 1. The initial concentrations were prepared by diluting 1000 mg L<sup>-1</sup> stock solution with pure distilled water [16].

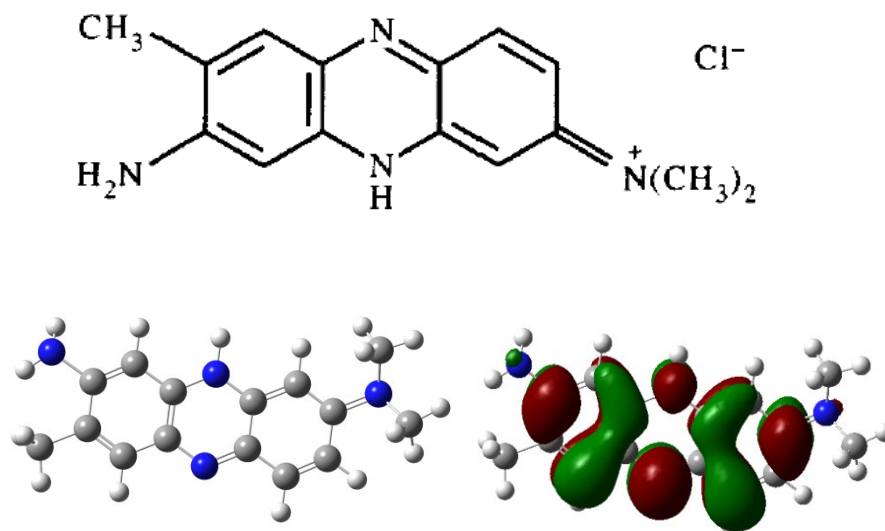


FIGURE 1. Chemical structure of NR.

## 2.3. Sample characterization

Chemical analysis of the Adilcevaz/Bitlis adsorbent was made using the Philips 2400 XRF instrument. Natural adsorbent is composed of 48.3% SiO<sub>2</sub>, 9.1% CaO, 7.2% MgO, 13.1% Al<sub>2</sub>O<sub>3</sub>, 9.4% Fe<sub>2</sub>O<sub>3</sub>, 0.9% TiO<sub>2</sub>, 1.3% Na<sub>2</sub>O, 2.9% K<sub>2</sub>O, 0.1% MnO and 0.1% P<sub>2</sub>O<sub>5</sub>. The surface area of the adsorbent was determined to be 37.118 (m<sup>2</sup>g<sup>-1</sup>) using the BET method (Quantachrome Nova 2200E Surface Area & Pore Size Analyzer). The pore diameter was determined to be 21.756 nm and 17.686 nm respectively by the BJH (Barrett-Joyner-Halenda) adsorption and desorption method based on the conventional Kelvin equation. By means

of BJH analysis, pore area, mean pore diameter and specific pore volume can be determined by using adsorption and desorption techniques. Pore size distribution of mesoporous solid material can also be obtained [17]. The cation exchange capacity (CEC) was determined to be 45 meq (100 g)<sup>-1</sup>. by the methylene blue adsorption method, which is a reliable and simple method for the presence and properties of the clay minerals in soil and rocks [18,19]. The cation exchange on montmorillonite and related smectites arise from the permanent structural charge resulting from the displacements in the crystal lattice [20]. Thermal analysis (TG-DTA) data were obtained by Rigaku 2.22E1 instrument with heating from room temperature to 1099 ° C temperature at a rate of 20 K min<sup>-1</sup>. XRD analysis was obtained using a Philips PW 1830-40 X-ray diffractometer with Ni-filtered Cu X-ray tube devices at 2-40 degrees. Feldspar, quartz, calcite, amorphous substance, smectite (montmorillonite), tridymite, mica mineral, mixed layered clay mineral, small amount of kaolinite and gypsum were determined in mineralogical structure. FT-IR analysis was performed using a Thermo Scientific Nicoletti S10 FT-IR spectrometer with a bandwidth of 400-4000 cm<sup>-1</sup>. The morphology of the natural adsorbent was provided using a scanning electron microscope (SEM, LEO 440 computer controlled digital).

#### 2.4. Methods

Batch adsorption experiments were performed in a temperature-controlled shaking water bath with a solution of 0.1 g of adsorbent in 10 ml aqueous solution of different concentrations of Neutral Red (NR) (25, 45, 65 and 85 mg L<sup>-1</sup>). The pH of the suspension was adjusted to approximately ( $\sim 7.1 \pm 0.1$ ) by dropwise addition of 0.1 mol L<sup>-1</sup> HCl or 0.1 mol L<sup>-1</sup> NaOH solutions using a WTW pH meter (Series 720, Germany). A constant agitation speed of 125 rpm was applied at a temperature of 298, 310 and 322 K. After the desired contact period, the samples were withdrawn from the mixture using a micropipette and centrifuged at 5000 rpm for 5 minutes. A contact time of 110 minutes was sufficient to achieve the adsorption equilibrium. After centrifugation, the supernatants were analyzed to determine the final concentration of Neutral Red (NR) by using a UV/VIS Spectrophotometer (PG Instruments T80) adjusted to a maximum absorbance of 533 nm. The

amount of dye adsorbed by the adsorbent was calculated according to the following Eq. 1. [21].

$$q_e = \frac{(C_0 - C_e)V}{m} \quad (1)$$

where “ $q_e$  is the amount of dye adsorbed ( $\text{mg g}^{-1}$ ).  $C_0$  and  $C_e$  are the initial and equilibrium liquid-phase concentrations of dye ( $\text{mg g}^{-1}$ ), respectively.  $V$  is the volume of the solution (L), and  $m$  is the weight of the sorbent used (g)”.

## 2.5. Adsorption Isotherms

Langmuir, Freundlich, Dubinin-Radushkevich, Tempkin, Redlich-Peterson, Sips and Koble-Corrigan nonlinear isotherm models were applied to explain the nature of the Neutral Red (NR) adsorption on the natural adsorbent (surface properties, mechanism of adsorption). All isotherm parameters were determined from a nonlinear regression analysis using a software program (Origin 8.0). The  $C_e$ - $q_e$  values obtained for dye adsorption on the natural adsorbent were applied to each nonlinear isotherm equation. Standard errors (S.E) were calculated for each isotherm model. S.E value is used to determine the isotherm that best fits the experimental data except for the correlation coefficient ( $R^2$ ). In addition, a chi-square value ( $\chi^2$ ), which is a statistical data required for the suitability of the obtained adsorption system, was calculated using the same software [15, 21]. The nonlinear regression method applied in computer operation minimizes the error distribution between the experimental data and the estimated isotherms [23]. The isotherm models are calculated from the equation presented in Table 1.

These parameters are determined in the following Eq.2 and 3.[24].

$$R^2 = \frac{\Sigma(q_{e,calc} - \overline{q_{e,exp}})^2}{\Sigma(q_{e,calc} - \overline{q_{e,exp}})^2 + \Sigma(q_{e,calc} - q_{e,exp})^2} \quad (2)$$

$$\chi^2 = \sum_{i=1}^N \frac{(q_{e,exp} - q_{e,calc})^2}{q_{e,calc}} \quad (3)$$

$q_{e,exp}$  (mmol g<sup>-1</sup>) is obtained from the batch experiment,  $q_{e,calc}$  (mmol g<sup>-1</sup>) is calculated from the isotherm for corresponding  $q_{e,exp}$ , and  $\overline{q_{e,exp}}$  is the average of  $q_{e,exp}$ . Also, N represents the number of observations in experimental data. In order to select the most suitable isotherm model, it is expected that R<sup>2</sup> is closer to 1,  $\chi^2$  and S.E are close to zero [25].

TABLE 1. Non-linear forms of the isotherm models.

| Isotherm                    | Equation   | Constants   | Reference |
|-----------------------------|--|---|-----------|
| <i>Langmuir</i>             | $q_e = \frac{q_M K_L C_e}{1 + K_L C_e}$                          | K <sub>L</sub> : Langmuir isotherm constant, (L g <sup>-1</sup> )   | [26]      |
| <i>Freundlich</i>           | $q_e = K_F C_e^{\frac{1}{n}}$                                    | K <sub>F</sub> : Freundlich isotherm constant, (L g <sup>-1</sup> )<br>n: The heterogeneity factor in the Freundlich model  | [27]      |
| <i>Dubinin-Radushkevich</i> | $q_e = q_M \exp(-K_{DR} E^2)$<br>$E = RT \ln(1 + \frac{1}{C_e})$ | K <sub>DR</sub> : D-R isotherm constant<br>E: Energy of adsorption<br>R: The ideal gas constant (8.314 (J mol <sup>-1</sup> K <sup>-1</sup> ))  | [28]      |
| <i>Temkin</i>               | $q_e = \frac{RT}{b_T} \ln(K_T C_e)$                              | K <sub>T</sub> : Temkin isotherm equilibrium binding constant (L g <sup>-1</sup> ) <sub>SEP</sub> <sup>[1]</sup><br>b <sub>T</sub> : Temkin isotherm constant<br>R: The ideal gas constant (8.314 (J mol <sup>-1</sup> K <sup>-1</sup> ))<br>T: The temperature (K) <sub>SEP</sub> <sup>[1]</sup> | [27]      |
| <i>Redlich-Peterson</i>     | $q_e = \frac{K_R C_e}{1 + a_R C_e^g}$                            | K <sub>R</sub> : Redlich-Peterson isotherm constant, (L g <sup>-1</sup> )<br>a <sub>R</sub> : Redlich-Peterson isotherm constant, (L g <sup>-1</sup> )<br>g: Redlich-Peterson isotherm constant   | [26]      |
| <i>Sips</i>                 | $q_e = \frac{K_S (a_S C_e)^{n_S}}{1 + (a_S C_e)^{n_S}}$          | K <sub>S</sub> : Sips isotherm constant, (L g <sup>-1</sup> )<br>a <sub>S</sub> : Sips isotherm constant, (L mg <sup>-1</sup> )<br>n <sub>S</sub> : Sips isotherm exponent <sub>SEP</sub> <sup>[1]</sup>  | [22]      |
| <i>Koble-Corrigan</i>       | $q_e = \frac{K C_e^n}{1 + a C_e^n}$                              | K: Koble-Corrigan isotherm constant (L <sup>n</sup> mg <sup>1-n</sup> g <sup>-1</sup> )<br>a: Koble-Corrigan isotherm constant (L mg <sup>-1</sup> ) <sub>SEP</sub> <sup>[1]</sup><br>n: Koble-Corrigan exponent  | [22]      |

### *2.5.1. Langmuir Isotherm*

This isotherm equation assumes that the adsorption takes place in certain homogeneous sites within the adsorbent. Furthermore, the Langmuir equation is based on the assumption that all adsorption sites are identical and energetically equivalent [26].

### *2.5.2. Freundlich Isotherm*

The Freundlich equation is an empirical equation used to describe heterogeneous systems characterized by the heterogeneity factor  $1/n$ . When  $n = 1$  the Freundlich equation is reduced to Henry's law. If  $1/n$  value is below 1, it shows normal adsorption. Conversely, if  $1/n$  is above 1, it indicates cooperative adsorption [27].

### *2.5.3. Dubinin–Radushkevich Isotherm*

This isotherm is usually applied by Gaussian energy distribution to express the adsorption mechanism on heterogeneous surfaces. If the energy value is below  $8 \text{ kJ mol}^{-1}$ , there are physical interactions in adsorption. Conversely, if the energy is above  $8 \text{ kJ mol}^{-1}$ , the adsorption mechanism can be described by chemical interactions. [28].

### *2.5.4. Tempkin Isotherm*

The model assumes that the adsorption heat (function of temperature) of all molecules in the layer will decrease linearly rather than logarithmic with coverage [27].

### *2.5.5. Redlich-Peterson Isotherm*

Redlich-Peterson isotherm is an empirical isotherm with three parameters. This isotherm model combines both the Langmuir and Freundlich equations and the adsorption mechanism is a hybrid mechanism and does not follow the ideal monolayer adsorption [26].

### *2.5.6. Sips Isotherm*

This isotherm is a combined form of Langmuir and Freundlich expressions derived to predict heterogeneous adsorption systems and

limit the increasing adsorbate concentration associated with the Freundlich isotherm model. At low adsorbate concentrations it is reduced to the Freundlich isotherm and at high concentrations it exhibits the monolayer adsorption capacity characteristic of the Langmuir isotherm [22].

#### *2.5.7. Koble–Corrigan isotherm model*

The Koble-Corrigan isotherm is a three-parameter equation that combines Langmuir and Freundlich isotherm models to represent equilibrium adsorption data [22]. It is usually applied to adsorbents having heterogeneous surfaces. In this equation, if  $n = 1$ , the isotherm is reduced to Langmuir isotherm. If  $n \ll 1$ , the isotherm is reduced to Freundlich isotherm [29].

### **2.6. Kinetics**

The pseudo-first-order kinetic model is used to elucidate the sorption in solid-liquid systems based on adsorbent adsorption capacity [30], which supposes that one of the pollutant molecules is trapped in one active site on the adsorbent surface [31]. According to the pseudo-second-order kinetic model, one of the adsorbate molecules is adsorbed on two sorption sites on the surface of the adsorbent. The Avrami kinetic model was first used for kinetic modeling of crystallization. However, it can also be used for other phase changes such as chemical reactions [32].

The intra-particle diffusion model is widely used to define the adsorption mechanism. If  $q_t$  vs  $t^{1/2}$  is linear and the line passes through the origin, intra-particle diffusion is included in the sorption process [33]. According to the Elovich equation, which interprets the sorption kinetics, the active solid sites are energetically heterogeneous and therefore represent different activation energies for chemical adsorption [34]. The equations corresponding to the pseudo-first-order and the pseudo-second-order kinetic model, Avrami kinetic model, Intra-particle diffusion model and Elovich equation are presented in Table 2.

TABLE 2. Non-linear forms of kinetic models.

| Equations                                       | Kinetic models          | Constants   | Reference |
|---|-------------------------|---|-----------|
| $q_t = q_e[1 - \exp(-k_1 t)]$                   | Pseudo-first order      | $k_1$ ( $\text{min}^{-1}$ ) is the pseudo-first-order rate constant<br>$t$ ( $\text{min}$ ) is the contact time   | [30]      |
| $q_t = \frac{k_2 q_e^2 t}{1 + k_2 q_e t}$       | Pseudo-second order     | $k_2$ ( $\text{g mg}^{-1} \text{min}^{-1}$ ) is the pseudo-second-order rate constant   | [35]      |
| $q_t = \frac{1}{\beta} \ln(1 + \alpha \beta t)$ | Elovich                 | $\alpha$ ( $\text{mg g}^{-1} \text{min}^{-1}$ ) is the initial adsorption rate<br>$\beta$ ( $\text{g mg}^{-1}$ ) is the desorption constant related to the extent of surface coverage and activation energy for chemisorption | [34]      |
| $q_t = q_e[1 - \exp(-k_{AV} t)^{n_{AV}}]$       | Avrami                  | $k_{AV}$ ( $\text{min}^{-1}$ ) is the Avrami kinetic constant<br>$n_{AV}$ is a constant which can be relational to the adsorption mechanism   | [32]      |
| $q_t = k_{id} \sqrt{t} + C_i$                   | Intraparticle diffusion | $k_{id}$ is intraparticle diffusion constant<br>$C_i$ is the intercept value (gives an indication about the thickness of boundary layer)  | [33]      |

## 2.7. Thermodynamic parameters

The values of free energy ( $\Delta G^\circ$ ), enthalpy ( $\Delta H^\circ$ ) and entropy ( $\Delta S^\circ$ ) were calculated using the following equations,

The apparent equilibrium constant ( $K_c'$ ) of the sorption is defined as

$$K_c' = \frac{C_{ad,eq}}{C_{eq}} \quad (4)$$

$$\ln K_c^o = -\frac{\Delta H^o}{RT} + \frac{\Delta S^o}{R} \quad (5)$$

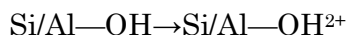
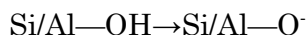
$$\Delta G^o = \Delta H^o - T\Delta S^o \quad (6)$$

where  $C_{ad,eq}$  is the concentration of dye on the adsorbent at equilibrium. This situation can be used instead of concentration with the aim of obtaining the standard thermodynamic equilibrium constant ( $K_c^o$ ) of the sorption system [36].  $R$  is the universal gas constant ( $8.314 \text{ J mol}^{-1} \text{ K}^{-1}$ ) and  $T$  is temperature (K).  $\Delta H^o$  and  $\Delta S^o$  values can be obtained from the slope and intercept of Van't Hoff plots of  $\ln K_c^o$  vs.  $1/T$  [37–39].  $\Delta G^o$  values are calculated using Eq. 6 for each temperature.

### 3. RESULTS AND DISCUSSION

#### 3.1. Surface properties of adsorbent

Clays display permanent structural charges on their surfaces and pH-dependent charges on the broken edges of the particles [40]. Phosphosilicate surface charge is due to heterovalent lattice substitutions and hydrolyzable aluminol ( $> \text{Al-OH}$ ) and silanol ( $> \text{Si-OH}$ ) edge site charge [41]. The proton adsorption / desorption properties of aluminol and silanol depend on the pH of the solution. Hydroxyl groups in the structure are the main reactive groups which interact with cationic dyes. The Si-OH and Al-OH groups in the clay structure are ionized as follows:



There is a  $\text{pH}_{pzc}$  where the sum of the negative charges is equal to the sum of the positive charges and the net charge on the surface is zero. The

$\text{pH}_{\text{pzc}}$  is a significant adsorbent factor that supports the adsorption of charged species and the influence of pH on the adsorption process [42]. As the pH increases, the number of negatively charged adsorption sites increases. Thus, the surface charge on the adsorbent becomes negative, and the electrostatic interaction between the cationic dye and the adsorbent increases. Whereas by decreasing the pH the surface of the positively charged adsorbent becomes attractive for anionic dyes [43]. The value of point zero charge ( $\text{pH}_{\text{pzc}}$ ) of the natural clay was determined to be 5.4 by the potentiometric titration method [44].



The site distributions modeled for aluminols and silanols for montmorillonite are described by Rozalen et al. (2009). According to the study, the  $\text{AlOH}^{+2}$  regions, which are in a very high saturation at around pH 4, decrease to pH 8 and  $\text{AlO}^-$  regions are formed at PH  $\sim 6.5$ . Silica areas remain neutral until pH  $\sim 7-7.5$  and start deprotonation at this point. Between pH 7 and pH 10, the negative surface charge is due to the addition of  $>\text{SiO}^-$  and  $>\text{AlO}^-$  sites. The silanol regions with PH  $> 10$  begin to become saturated and the increases in negative surface charge include aluminol regions [41]. The Adilcevaz clay has a negative surface charge at the pH value studied ( $\sim 7.1 \pm 0.1$ ).

### 3.2. Characterization of the adsorbent

FT-IR analysis has been used as an effective method to identify the functional groups responsible for adsorption. Figure 2 shows the FT-IR spectrum of the natural adsorbent before and after the Neutral Red (NR) adsorption process and shows some characteristic variations in the FT-IR spectrum of the adsorbent after dye adsorption. Some peaks appear to have disappeared or replaced, and in some cases new peaks appear. NR molecules interact with the functional groups of the adsorbent, causing the observed changes in the spectrum [45].

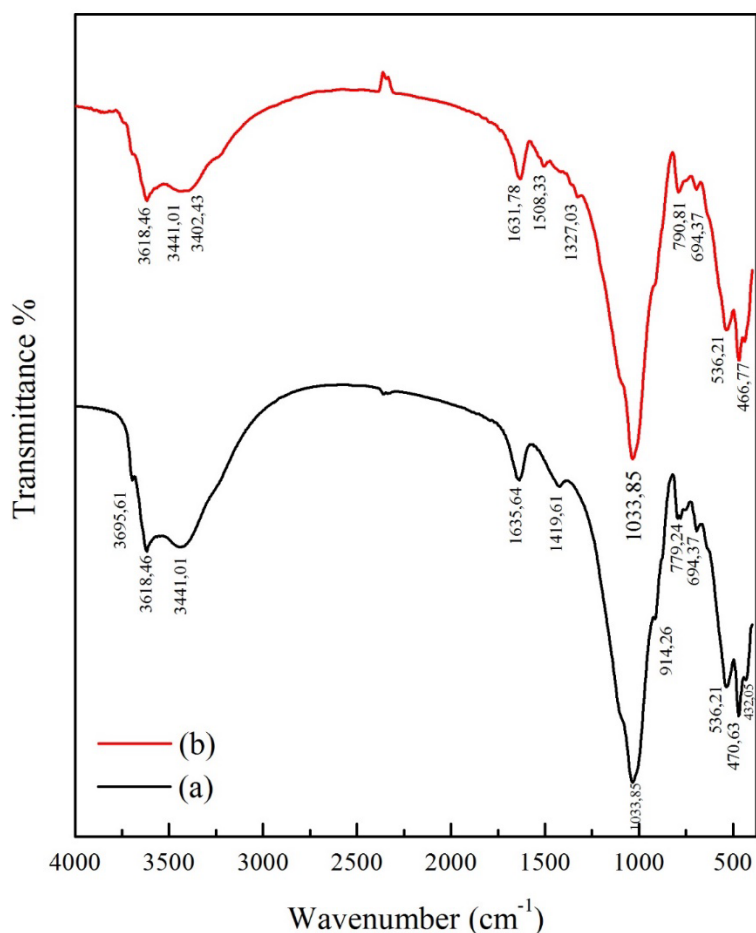


FIGURE 2. FT-IR spectra before (a) and after (b) NR adsorption.

The bands at 3695 and 3618 cm<sup>-1</sup> confirm the presence of kaolinite [46]. The peaks of surface hydroxyl groups (Si-Si-OH or Al-Al-OH) stretching vibrations were observed at 3695.61 and 3618.46 cm<sup>-1</sup>. The peaks of the stretching vibration of adsorbed water molecules are observed at 3441.01 and 1635.64 cm<sup>-1</sup>, respectively. The characteristic bands of 1419.61 cm<sup>-1</sup> and 1033.85 cm<sup>-1</sup> are respectively associated with calcite and clay minerals or quartz (Fig. 2a) [47]. After NR adsorption onto adsorbent, shifts in wavenumber of adsorbed water and calcite were observed, and a new peak appeared in the 1508.33 cm<sup>-1</sup> band. At 1419 cm<sup>-1</sup> the peak is due

to the stretching vibration of the C-O associated with the carboxyl group. This group may act as a proton donor and therefore may contain deprotonated hydroxy and carboxyl groups in coordination with the positive dye. When NR is dissolved in water, it will be positively charged and adsorbed [45,48,49]. Figure 2 shows that the natural adsorbent contains functional groups such as OH, COO<sup>-</sup> and CO and that these groups are responsible for interacting with the dye.

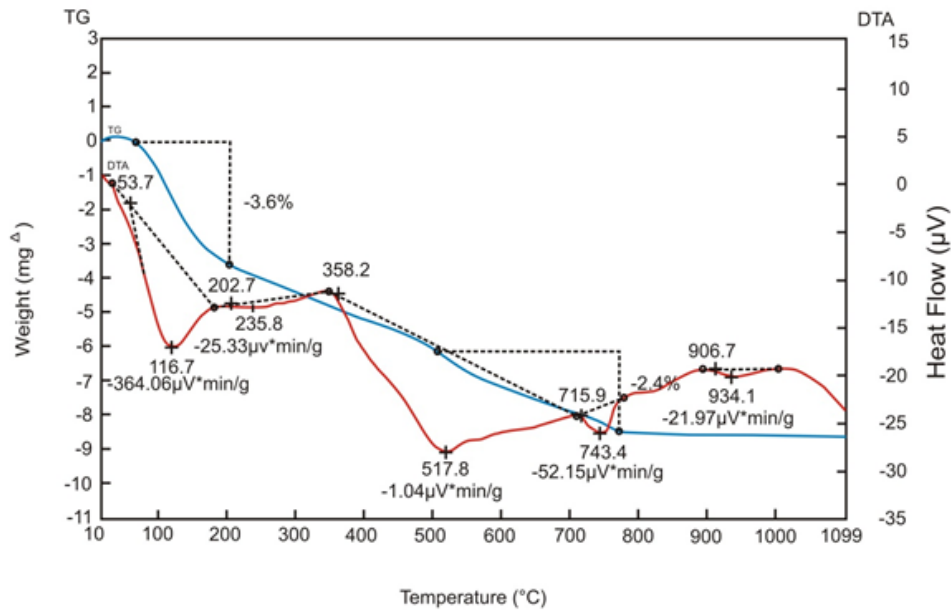


FIGURE 3. Thermal analysis diagram of the Adilcevaz clay sample.

The thermal analysis diagram of the clay sample is shown in Figure 3. Due to the dehydration of clay minerals, a peak at 116.7 °C was observed. The weight loss corresponding to 3.6% for the sample is due to the removal of physically bound water. This peak is probably due to mixed layer smectite presence [50]. The second broad endothermic event occurs at 400-600 °C and there is a weight loss of 2.4% for clay. This peak is probably mainly due to the removal of the OH group of kaolinite [46,51].

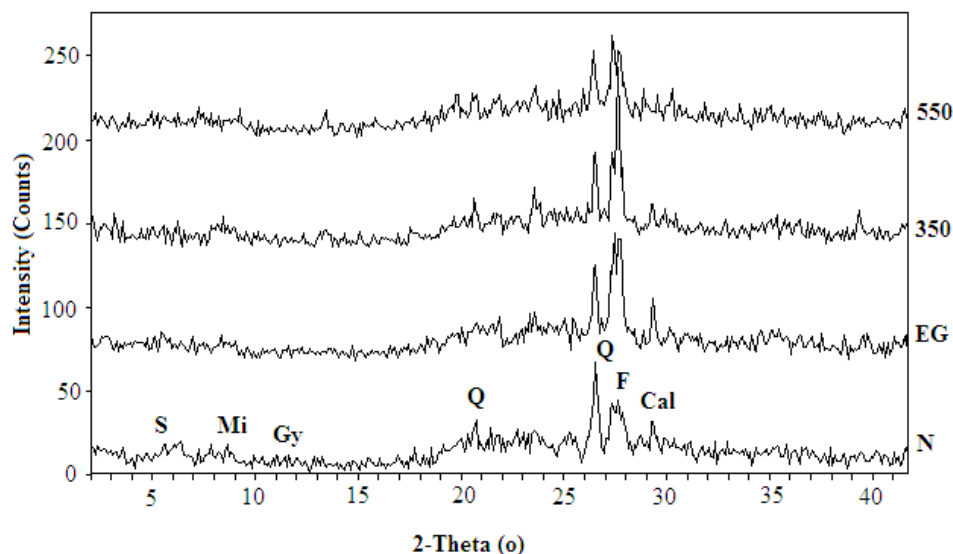


FIGURE 4. XRD pattern of Adilcevaz clay sample.

(S: Smectite group clay; Mi: Mica; Gy: Gypsum; Q: Quartz; F: Feldspar; Cal: Calcite)

X-ray diffraction patterns showed the presence of smectite group clay minerals at 15.7965 Å and 13.9856 Å (Fig 4). Also, mica at 10.1638 Å, gypsum at 7.6420 Å, quartz at 4.2903 Å and 3.3572 Å, feldspar at 3.2234 Å and calcite reflections at 3.0445 Å were observed. In the clay fraction, smectite was detected in the ethylene glycol treated diffraction at (17.1451 Å). In addition, on the diffractogram (Fig. 4), there were observed reflections of kaolinite minerals at 3.5573 Å (001) and 7.2193 Å (002), confirming the presence small amount of kaolinite [52–54]. These reflections remained unchanged with the treatments, but were destroyed after heating to 550 ° C.

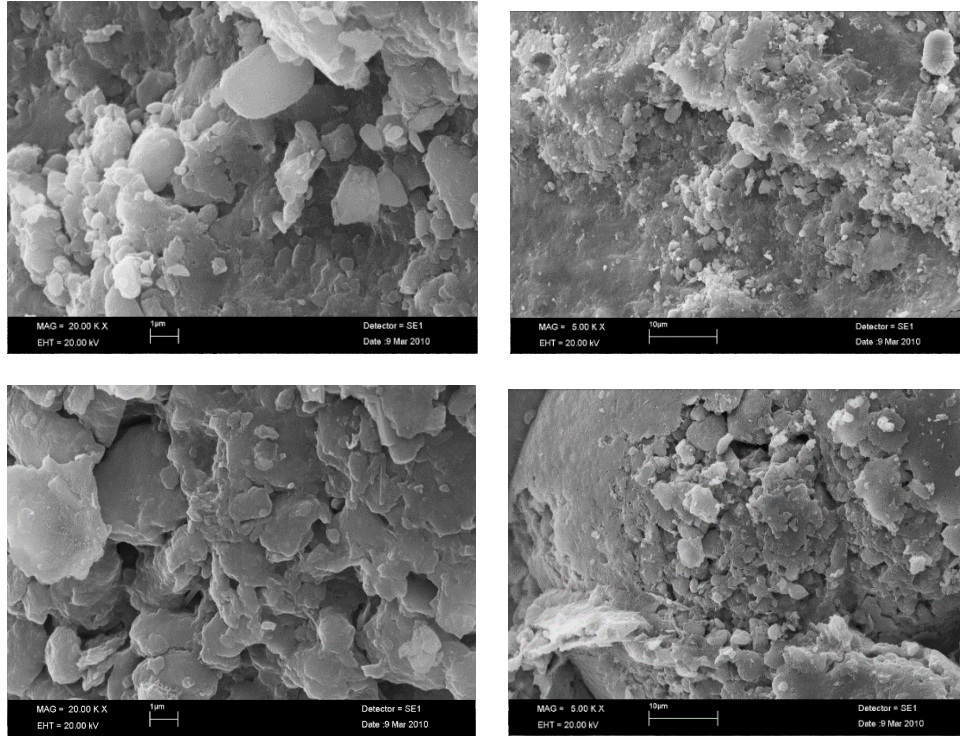


FIGURE 5. SEM images of Adilcevaz clay sample.

The SEM image of natural clay is shown in Figure 5. The original sample showed a typical scanning electron micrograph of the smectic clay. It can be seen that the Adilcevaz clay have advanced textural properties (for example, surface area and porosity), flat sheet and spongy structure [55].

### 3.3. Effect of initial dye concentration with contact time

It is essential to determine the effect of the initial dye concentration as it provides the initial impulse needed to overcome the mass transfer resistance through the sol-sorbent interface of the dye. Figure 6 shows the effect of the initial dye concentration ( $25\text{-}85\text{ mg L}^{-1}$ ) as a function of contact time (3-275 min) at the removal of NR by the natural adsorbent.

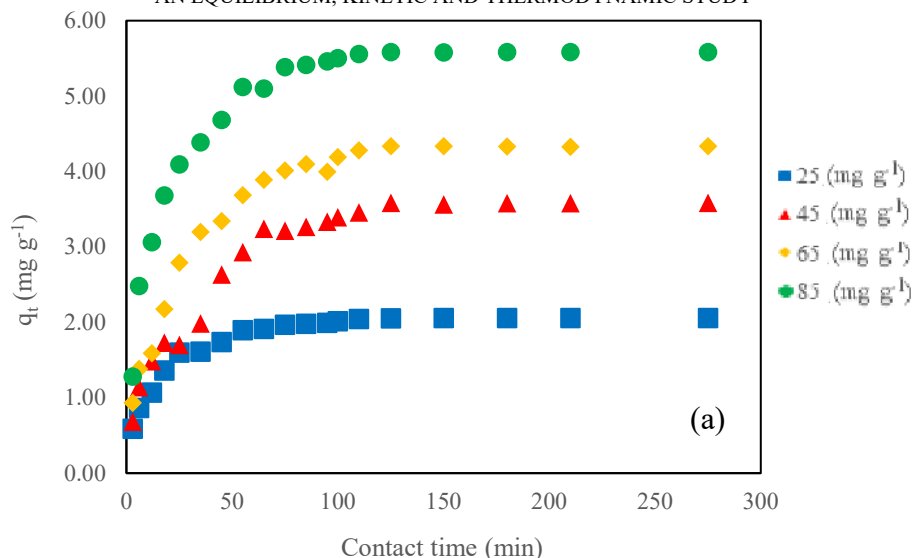


FIGURE 6. Effect of contact time and initial concentration for NR adsorption on Adilcevaz clay sample at 298 K.

As can be seen from Fig.6, with increasing concentration for dye adsorption, the adsorption initially increases and then reaches equilibrium. To ensure equilibrium saturation, the experiments were continued for up to 275 minutes. The first rapid uptake may be due to the external diffusion of the dye to the adsorbent surface. As time progresses, slower uptake may be attributed to slower intracellular diffusion due to lower dye concentration and constant adsorbent amount in the adsorption system [34].

### 3.4. Effect of temperature

It is important to examine the temperature effect for the adsorption process. In addition to affecting the equilibrium capacity of adsorption, it also describes the exothermic and / or endothermic properties of the adsorption process. The constant amounts of natural adsorbent and different initial concentrations of the dye (25-85 mg L<sup>-1</sup>) were studied. It was observed that dye adsorption increased with increasing temperature for all dye concentrations and is shown in Fig. 7 for C<sub>0</sub> = 65 mg L<sup>-1</sup>.

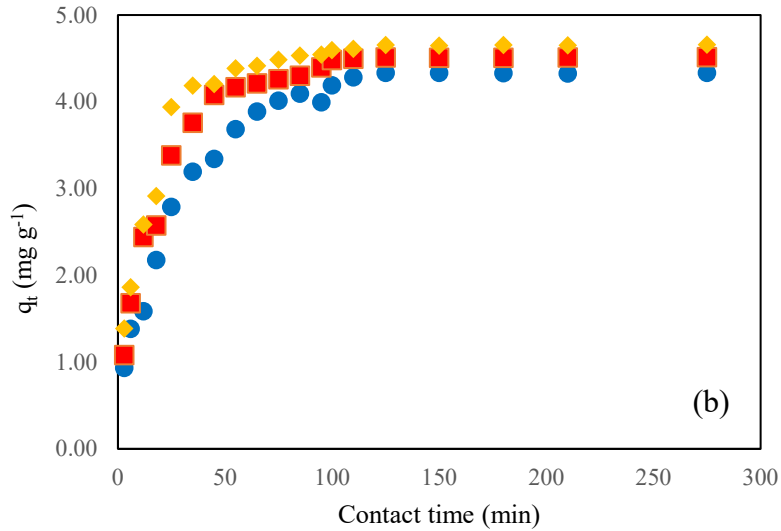


FIGURE 7. The effect of temperature on the adsorption of NR on Adilcevaz clay ( $C_0 = 65 \text{ mg L}^{-1}$ ).

This can be explained by the increase in the mobility of the NR reaching the surface of the adsorbent with increasing temperature. In addition, the adsorption rate is also affected because the temperature changes the molecular interactions and the solubility of the dye [34].

### 3.5. Adsorption isotherms

Nonlinear diagrams of isotherm models for dye (NR) adsorption on the natural adsorbent are given in Figure 8a and b. The values of the two-parameter (Table 3a) and three-parameter (Table 3b) isotherm models are listed.

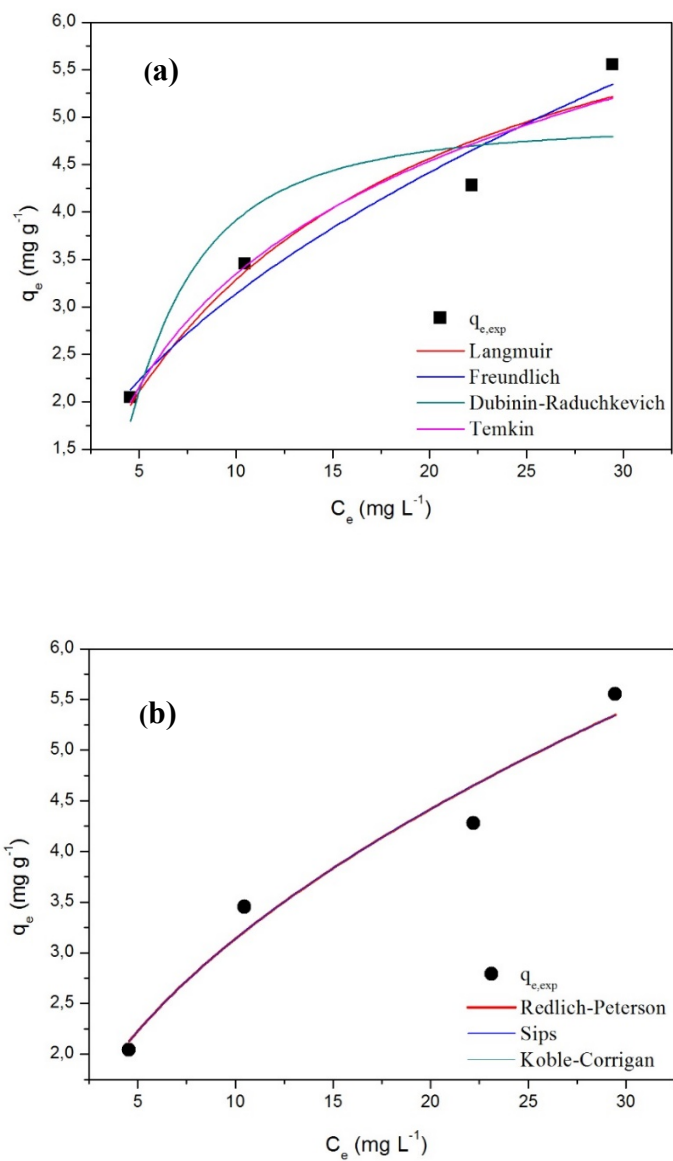


FIGURE 8. Comparison of adsorption isotherm models for the sorption of NR on Adilcevaz clay sample at 298 K; (a) two-parameter isotherms; (b) three-parameter isotherms.

In Figure 8, the correlation between the amount of NR dye adsorbed on the surface of the clay and the dye concentration of the aqueous phase at equilibrium is observed [56].

TABLE 3a. Values of the parameters of the two-parameter models.

| Isotherm/Model       |                             | 298 K  |         | 310 K  |        | 322 K  |        |
|----------------------|-----------------------------|--------|---------|--------|--------|--------|--------|
|                      |                             | Value  | S.E     | Value  | S.E    | Value  | S.E    |
| Langmuir             | $q_m$ (mg g <sup>-1</sup> ) | 7.4734 | 1.2902  | 7.2136 | 1.1111 | 6.6711 | 0.9858 |
|                      | $K_L$                       | 0.0784 | 0.0329  | 0.1116 | 0.0464 | 0.1965 | 0.9490 |
|                      | $R_L$                       | 0.3378 | -       | 0.2638 | -      | 0.1691 | -      |
|                      | $R^2$                       | 0.9203 | -       | 0.9033 | -      | 0.8445 | -      |
|                      | $\chi^2$                    | 0.1727 | -       | 0.2256 | -      | 0.3877 | -      |
| Freundlich           | $K_F$                       | 1.0073 | 0.2490  | 1.2877 | 0.3636 | 1.7415 | 0.5098 |
|                      | $1/n$                       | 0.4935 | 0.3356  | 0.4430 | 0.4945 | 0.3690 | 0.7707 |
|                      | $R^2$                       | 0.9431 | -       | 0.8995 | -      | 0.8369 | -      |
|                      | $\chi^2$                    | 0.1232 | -       | 0.2354 | -      | 0.4065 | -      |
| Dubinin-Radushkevcih | $q_m$ (mg g <sup>-1</sup> ) | 4.9359 | 1.0373  | 4.0125 | 1.3259 | 5.3652 | 0.8216 |
|                      | $K_{D-R}$                   | 1.1578 | 10.1885 | 1.0006 | 1.0167 | 5.3721 | 2.6045 |
|                      | $E_{D-R}$                   | 4.7006 | 20.6810 | 2.1523 | 0.0012 | 5.3021 | 1.8549 |
|                      | $R^2$                       | 0.4960 | -       | 0.5129 | -      | 0.6032 | -      |
|                      | $\chi^2$                    | 1.0930 | -       | 7.0322 | -      | 0.9893 | -      |
| Temkin               | $b_T$                       | 1.4438 | 0.2746  | 1.5161 | 0.2942 | 1.8078 | 0.3432 |
|                      | $K_T$                       | 0.7032 | 0.2650  | 0.9185 | 0.3951 | 1.7948 | 1.2348 |
|                      | $R^2$                       | 0.9268 | -       | 0.9151 | -      | 0.8544 | -      |
|                      | $\chi^2$                    | 0.1585 | -       | 0.1988 | -      | 0.3629 | -      |

TABLE 3b. Values of the parameters of the three-parameter models.

| Isotherm/Model   |                             | 298 K     |        | 310 K     |         | 322 K    |        |
|------------------|-----------------------------|-----------|--------|-----------|---------|----------|--------|
|                  |                             | Value     | S.E    | Value     | S.E     | Value    | S.E    |
| Redlich-Peterson | $K_R$                       | 4.3837    | 0.0001 | 1.1328    | 3.1689  | 1.8118   | 5.7604 |
|                  | $a_R$                       | 4.3453    | 0.0001 | 0.3189    | 2.1249  | 0.4506   | 2.9740 |
|                  | $g$                         | 0.5068    | 0.8289 | 0.8079    | 1.0062  | 0.8551   | 0.9557 |
|                  | $R^2$                       | 0.8869    | -      | 0.8160    | -       | 0.6985   | -      |
|                  | $\chi^2$                    | 0.2465    | -      | 0.4311    | -       | 0.7516   | -      |
| Sips             | $q_m$ (mg g <sup>-1</sup> ) | 4.5212    | 9.9016 | 8.4620    | 13.9076 | 6.4969   | 4.6495 |
|                  | $a_S$                       | 4.6577E-6 | 0.0021 | 7.5430E-4 | 0.3219  | 2.900E-4 | 0.3371 |
|                  | $n_S$                       | 0.4975    | 0.9312 | 0.8360    | 1.2992  | 1.0569   | 1.6393 |
|                  | $R^2$                       | 0.8861    | -      | 0.8081    | -       | 0.6891   | -      |
|                  | $\chi^2$                    | 0.2469    | -      | 0.4497    | -       | 0.7751   | -      |
| Koble-Carrigan   | $a_{KC}$                    | 1.0072    | 0.3504 | 0.9744    | 1.4775  | 1.2308   | 2.1861 |
|                  | $b_{KC}$                    | 1.5388    | 0.1139 | 0.1152    | 0.0793  | 0.1902   | 0.2351 |
|                  | $n_{KC}$                    | 0.4935    | 0.1139 | 0.8366    | 1.2865  | 1.0657   | 1.6351 |
|                  | $R^2$                       | 0.8863    | -      | 0.8081    | -       | 0.6891   | -      |
|                  | $\chi^2$                    | 0.2465    | -      | 0.4497    | -       | 0.7751   | -      |

The  $R^2$  value determined from the Langmuir equation is 0.9203, the  $\chi^2$  value is 0.1727 at 298 K. The  $q_m$  value was determined to be 7.4734, but SE was found to be quite high. The  $R_L$  values at temperatures of 298, 310 and 322 K were found to be 0.3378, 0.2638 and 0.1691, respectively. According to the Langmuir isotherm, it has been verified that the adsorption of NR on the natural adsorbent is favorable for the conditions of this study [57]. As seen from Table 3a, the Freundlich isotherm model has higher regression coefficient (0.9431) and lower SE (0.2490) and  $\chi^2$  (0.1232) values than the other two parameter isotherm models. In addition, the  $K_F$  and  $1/n$  values were calculated as 1.0073 and 0.4935, respectively.  $1/n$  value between 0 and 1 showed that NR was easily adsorbed by the natural sorbent. The D-R adsorption isotherm did not provide good data for this study ( $R^2 = 0.4960$ ). As the adsorption energy (E) values are below 8 kJ mol<sup>-1</sup> at all the studied temperatures, it is

understood that the adsorption mechanism is the combination of electrostatic interaction and physical adsorption [44].

The correlation coefficient obtained from Tempkin isotherm at 298 K is 0.9268. The low value (1.4438) of the Tempkin constant  $b_T$  ( $\text{J mol}^{-1}$ ) shows a weak adsorbate-adsorbent interaction [24].

The "g" constant of the Redlich-Peterson isotherm approximates Henry's law (as the exponent "g" is all close to one) at low concentrations and Freundlich's isotherm behavior at high concentrations (as the exponent tends to zero) [58] [59]. In Table 3b, the exponential "g" value for dye adsorption on the adsorbent at 298 K can be assumed to be close to zero ( $g = 0.5068$ ).

If  $n_s = 1$ , a dimensionless heterogeneity factor in the Sips isotherm equation, this equation is reduced to the Langmuir equation and indicates that the adsorption process is homogenous [60]. It has been verified that adsorption is heterogeneous from the Sips isotherm constant (0.4975) in Table 3b. Also, the Koble-Corrigan exponent was calculated to be 0.4935. This is attributed to the suitability of the adsorption process to the Freundlich isotherm.

### 3.6. Adsorption kinetics

The kinetic studies, which are very significant in understanding the adsorption mechanism, have been investigated as a function of contact time for different initial NR dye concentrations.

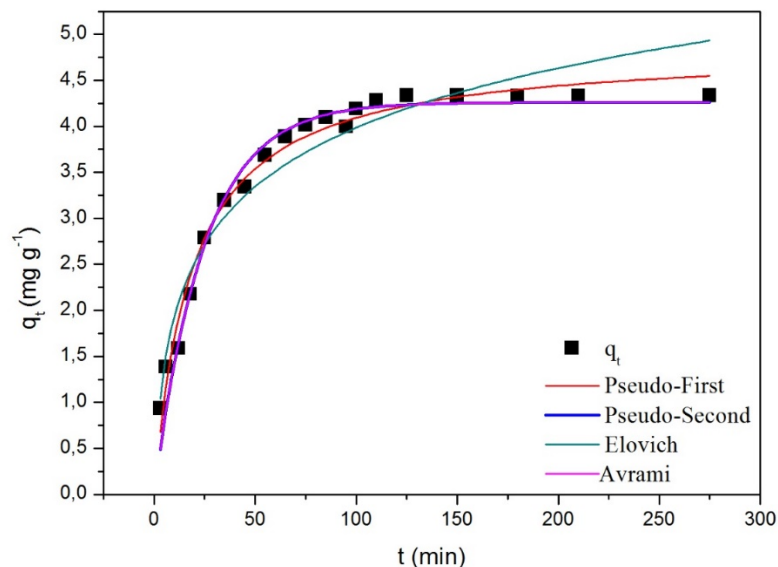


FIGURE 9. Experimental data of adsorption kinetic and non-linear fitting of pseudo-first order, pseudo-second order, Elovich, and Avrami models for NR on Adilcevaz clay sample at 298 K

Different kinetic models such as pseudo-first order, pseudo-second-order, Elovich model, Avrami model, and Weber and Morris intraparticle diffusion model were used in the evaluation of experimental data. Statistical analysis tests were conducted to evaluate the fitness of the model and to determine the suitability of the model. Higher  $R^2$  and lower error function values are referred to as better model fitting. Equations of model are given in chapter 2. The results of the modeling data for the NR adsorption on the natural adsorbent are presented in Table 4.

TABLE 4. Kinetic parameters for the adsorption of NR dye on Adilcevaz clay sample ( $C_0 = 65 \text{ mg L}^{-1}$ ).

| Kinetic Models      |  | Adilcevaz     |               |               |
|---------------------|--|---------------|---------------|---------------|
|                     |  | 298 (K)       | 308 (K)       | 318 (K)       |
|                     | $q_e \text{ (exp)} \text{ (mg g}^{-1}\text{)}$     | <b>4.2810</b> | <b>4.4970</b> | <b>4.6120</b> |
| Pseudo-first order  | $q_{e, \text{(cal)}} \text{ (mg g}^{-1}\text{)}$   | 4.8543        | 4.4260        | 4.5672        |
|                     | $k_1 \text{ (min}^{-1}\text{)}$                    | 0.0110        | 0.0595        | 0.0718        |
|                     | $\chi^2$   | 0.0243        | 0.0269        | 0.0352        |
|                     | $R^2$  | 0.9806        | 0.9734        | 0.9659        |
| Pseudo-second order | $q_{e, \text{(cal)}} \text{ (mg g}^{-1}\text{)}$   | 4.2884        | 4.9466        | 4.7859        |
|                     | $k_2 \text{ (g mg}^{-1} \text{ min}^{-1}\text{)}$  | 0.0110        | 0.0175        | 0.0215        |
|                     | $\chi^2$   | 0.0243        | 0.0180        | 0.0270        |
|                     | $R^2$  | 0.9906        | 0.9938        | 0.9738        |
| Elovich             | $A \text{ (mg g}^{-1} \text{ min}^{-1}\text{)}$    | 0.6324        | 1.3930        | 2.3036        |
|                     | $B \text{ (g mg}^{-1}\text{)}$                     | 1.0587        | 1.1917        | 1.2671        |
|                     | $\chi^2$   | 0.0777        | 0.1031        | 0.1268        |
|                     | $R^2$  | 0.9381        | 0.9075        | 0.8776        |
| Avrami              | $q_{e, \text{(cal)}} \text{ (mg g}^{-1}\text{)}$   | 4.2607        | 4.4260        | 4.5672        |
|                     | $k_{AV} \text{ (min}^{-1}\text{)}$                 | 0.2014        | 0.2440        | 0.2681        |
|                     | $n_{AV}$   | 0.2014        | 0.2440        | 0.2681        |
|                     | $\chi^2$   | 0.0353        | 0.0315        | 0.0374        |
| Intraparticle       | $k_{id} \text{ ((mg g}^{-1}\text{h}^{1/2}\text{)}$ | <b>0.1911</b> | <b>0.1130</b> | <b>0.0799</b> |
| Diffusion           | $C_o$  | 2.3177        | 3.3030        | 3.7863        |
| Model               | $R^2$  | 0.9573        | 0.9205        | 0.9708        |

The pseudo-first-order kinetic model, which has an expression based on the adsorption capacity of the adsorbent, is among the kinetic models generally applied [61]. The results in Table 4 show that there is a considerable difference between the calculated values ( $q_{e \text{ (calc)}}$ ) and the experimental values ( $q_{e \text{ (exp)}}$ ). Compared to other model parameters, low

correlation coefficient values and relatively high  $\chi^2$  values indicate that this model is not applicable for NR adsorption on the natural adsorbent.

The pseudo-second-order kinetic model helps predict the adsorption rate of a given adsorption system. The adsorption ratio is based on the assumption that the number of bonding areas on the adsorbent is proportional to the square [62]. Equation and corresponding constants are presented in Table 2. From the values in Table 4, it is observed that the values of  $q_e$  (calc) and  $q_e$  (exp) are almost similar. In the same way,  $R^2$  values are close to 1 and  $\chi^2$  values are lower. Therefore, the NR adsorption on the natural adsorbent follows the pseudo second order kinetic model sufficiently. Figure 9 depicts the corresponding model graph of NR at 298 K. For all temperatures, this model emphasizes the potential applicability to experimental kinetic data. As the initial dye concentration increases, the rate coefficient  $k_2$  of the pseudo-second order decreases (these values are not given in the Table 4). This shows a decrease in the electrostatic interaction on site as the initial concentration increases, thereby reducing the dye affinity toward natural adsorbent [63].

The Elovich model is a kinetic model based on adsorption capacity, which assumes that the adsorption mechanism is chemical or physical adsorption [64]. The Elovich equation and the characteristic parameter values are presented in Table 4, respectively. The fact that the  $\chi^2$  value is significantly lower at 298 K, but this value is quite high for the other two temperatures, as well as the low values of the correlation coefficients at all temperatures, makes the suitability of this model for experimental data questionable. [34]. It appears that  $B$ , a constant associated with the extension of surface coverage, decreases with an increase in the initial adsorbate concentration (these values are not given in the Table 4). The surface area of the adsorbent is not very high, so the adsorption of NR may be through functional groups.

For the kinetic evaluation of the adsorption process, the Avrami kinetic model was also used. The lower  $\chi^2$  and  $R^2$  values obtained for the Avrami kinetic model confirm that this kinetic model does not define the NR uptake kinetics on the natural adsorbent.

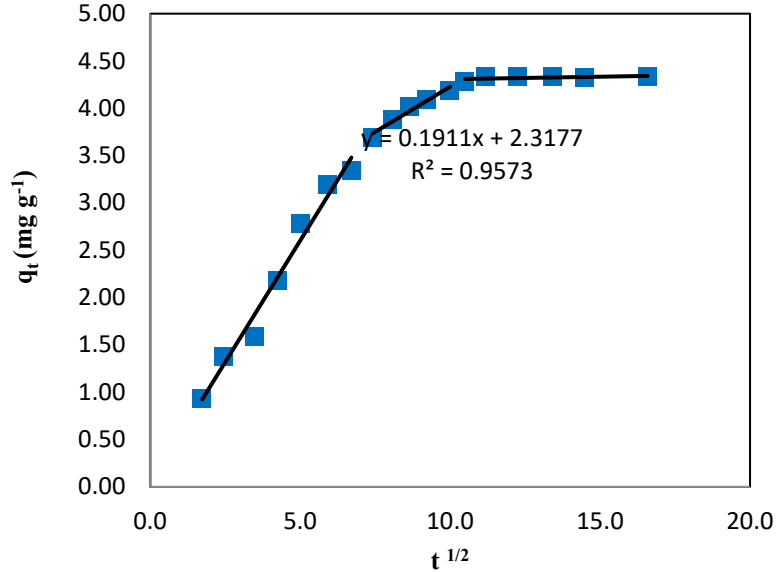


FIGURE 10. Intra-particle diffusion plots for NR adsorption on Adilcevaz clay sample at 298 K.

The intraparticle diffusion plot is the plot of amount sorbed per unit weight of sorbent,  $q_t$  (mg g<sup>-1</sup>) versus square root of time,  $t^{1/2}$  is shown in Figure 10.

The intraparticle diffusion model clearly demonstrates the multiple adsorption steps and this plot didn't pass through the origin, indicating that intra-particle diffusion is not the only rate-limiting step in the adsorption process [63,64]

### 3.7. Adsorption thermodynamic

Thermodynamic parameters such as enthalpy ( $\Delta H^\circ$ ), entropy ( $\Delta S^\circ$ ), and Gibbs free energy ( $\Delta G^\circ$ ) are used for a better understanding of the effect of temperature effect on dye adsorption in adsorbents. Table 5 shows thermodynamic parameters for NR dye adsorption on natural adsorbent.

TABLE 5. Thermodynamic parameters for NR dye adsorption on Adilcevaz clay sample.

| C <sub>o</sub><br>(mg L <sup>-1</sup> ) | ΔH°<br>(kJ mol <sup>-1</sup> ) | ΔS°<br>(J mol <sup>-1</sup> K <sup>-1</sup> ) | ΔG°<br>(kJ mol <sup>-1</sup> ) |         |         |
|---|--------------------------------|---|--------------------------------|---------|---------|
|   |                                |   | 298 (K)                        | 310 (K) | 322 (K) |
| 25                                      | 263.51                         | 1.0595  | -3.7234                        | -4.2433 | -5.5001 |
| 45                                      | 333.83                         | 1.2633  | -2.9596                        | -3.9628 | -5.0576 |
| 65                                      | 113.86                         | 0.4622  | -1.6281                        | -2.0845 | -2.3910 |
| 85                                      | 119.35                         | 0.4759  | -1.5722                        | -1.9052 | -2.3650 |

The obtained ΔH° values are in the range of 333.83 kJ mol<sup>-1</sup> to 113.86 kJ mol<sup>-1</sup> at various initial dye concentrations. A positive sign indicates that the process is endothermic in nature. This behavior may be due to an increase in the diffusion rate of the adsorbate throughout the inner boundary of the outer boundary layer and the adsorbents [65,66]. The ΔS° value obtained is positive at all initial dye concentrations, indicating that the degree of freedom during adsorption increases at the solid-liquid interface. In addition, the positive value indicates the affinity of the adsorbate to the solid-liquid interface, which reflects the adsorbent affinity [67,68]. The negative value of ΔG° indicates that the adsorption process is spontaneous. The obtained ΔG° values are lower than 20 kJ mol<sup>-1</sup>; this also supports the fact that the adsorption process follows the physisorption mechanism [69].

#### 4. CONCLUSION

The natural Adilcevaz clay is a good alternative adsorbent to remove the NR dye from the aqueous solutions. When this adsorbent is suspended in water, it interacts with the dye at the solid / liquid interface. Equilibrium isotherm modeling of NR adsorption was performed and the data best fit the Freundlich isotherm model. Five kinetic models were used to adjust the adsorption and the best fit was provided by the pseudo-second kinetic model; however, the intra-particle diffusion model has multiple linear regions, which suggest that the adsorption can also be followed by multiple adsorption rates. The maximum capacity of this adsorbent

which is cheap and does not cause secondary pollution was determined as  $4.2810 \text{ mg g}^{-1}$  from the experimental data.  $\Delta H^\circ$  of adsorption process; Thermodynamic parameters such as  $\Delta S^\circ$  and  $\Delta G^\circ$  were determined. The enthalpy changes ( $\Delta H^\circ$ ) indicate that the adsorption follows endothermic processes, and the enthalpy magnitude is compatible with the physical interaction of an adsorbent with an adsorbate.

#### **Authors' Contribution Statement**

Ali Rıza Kul: Conceptualization, Formal analysis, Writing - original draft, Writing - review & editing. Eda Gökırmak Söğüt: Formal analysis, Writing - original draft, Writing - review & editing. Necla Çalışkan Kılıç: Conceptualization, Formal analysis, Writing - original draft, Writing - review & editing.

#### **Declaration of Competing Interests**

The authors declare that they have no known competing financial interests or personal relationships that could have appeared to influence the work reported in this paper.

## REFERENCES

- [1] Bendaho, D., Driss, T.A., Bassou, D., Adsorption of acid dye onto activated Algerian clay, *Bulletin of the Chemical Society of Ethiopia*, 31 (1) (2017), 51–62. <https://doi.org/10.4314/bcse.v31i1.5>.
- [2] Benkhaya, S., M' rabet, S., El Harfi, A., A review on classifications, recent synthesis and applications of textile dyes, *Inorganic Chemistry Communications*, 115 (2020), <https://doi.org/10.1016/j.inoche.2020.107891>.
- [3] Zhang, J., Shi, Q., Zhang, C., Xu, J., Zhai, B., Zhang, B., Adsorption of Neutral Red onto Mn-impregnated activated carbons prepared from *Typha orientalis*, *Bioresource Technology*, 99 (18) (2008), 8974–8980. <https://doi.org/10.1016/j.biortech.2008.05.018>.
- [4] Iram, M., Guo, C., Guan, Y., Ishfaq, A., Liu, H., Adsorption and magnetic removal of neutral red dye from aqueous solution using Fe<sub>3</sub>O<sub>4</sub> hollow nanospheres, *Journal of Hazardous Materials*, 181 (1–3) (2010), 1039–1050. <https://doi.org/10.1016/j.jhazmat.2010.05.119>.
- [5] Wong, C.W., Barford, J.P., Chen, G., McKay, G., Kinetics and equilibrium studies for the removal of cadmium ions by ion exchange resin, *Journal of Environmental Chemical Engineering*, 2 (1) (2014), 698–707.

- <https://doi.org/10.1016/j.jece.2013.11.010>.
- [6] Alvarez, M.T., Crespo, C., Mattiasson, B., Precipitation of Zn(II), Cu(II) and Pb(II) at bench-scale using biogenic hydrogen sulfide from the utilization of volatile fatty acids, *Chemosphere*, 66 (9) (2007), 1677–1683. <https://doi.org/10.1016/j.chemosphere.2006.07.065>.
- [7] Gupta, V.K., Jain, R., Nayak, A., Agarwal, S., Shrivastava, M., Removal of the hazardous dye-Tartrazine by photodegradation on titanium dioxide surface, *Materials Science and Engineering C*, 31 (5) (2011), 1062–1067. <https://doi.org/10.1016/j.msec.2011.03.006>.
- [8] Qiu, Y.R., Mao, L.J., Removal of heavy metal ions from aqueous solution by ultrafiltration assisted with copolymer of maleic acid and acrylic acid, *Desalination*, 329 (2013), 78–85. <https://doi.org/10.1016/j.desal.2013.09.012>.
- [9] Mondal, N.K., Das, K., Das, B., Sadhukhan, B., Effective utilization of calcareous soil towards the removal of methylene blue from aqueous solution, *Clean Technologies and Environmental Policy*, 18 (3) (2016), 867–881. <https://doi.org/10.1007/s10098-015-1065-z>.
- [10] Shen, Z., Jin, F., Wang, F., McMillan, O., Al-Tabbaa, A., Sorption of lead by Salisbury biochar produced from British broadleaf hardwood, *Bioresource Technology*, 193 (2015), 553–556. <https://doi.org/10.1016/j.biortech.2015.06.111>.
- [11] Afroz, S., Sen, T.K., Ang, M., Nishioka, H., Adsorption of methylene blue dye from aqueous solution by novel biomass Eucalyptus sheathiana bark: equilibrium, kinetics, thermodynamics and mechanism, *Desalination and Water Treatment*, 57 (13) (2016), 5858–5878. <https://doi.org/10.1080/19443994.2015.1004115>.
- [12] Gürses, A., Doğar, Ç., Yalçın, M., Açikyildiz, M., Bayrak, R., Karaca, S., The adsorption kinetics of the cationic dye, methylene blue, onto clay, *Journal of Hazardous Materials*, 131 (1–3) (2006), 217–228. <https://doi.org/10.1016/j.jhazmat.2005.09.036>.
- [13] Fatiha, M., Belkacem, B., Adsorption of methylene blue from aqueous solutions using natural clay, *J. Mater. Environ. Sci*, 7 (1) (2016), 285–292.
- [14] Ajala, O.J., Nwosu, F.O., Ahmed, R.K., Adsorption of atrazine from aqueous solution using unmodified and modified bentonite clays, *Applied Water Science*, 8 (7) (2018), 214. <https://doi.org/10.1007/s13201-018-0855-y>.
- [15] Caliskan, N., Sogut, E.G., Savran, A., Riza Kul, A., Kubilay, S., Removal of Cu(II) and Cd(II) ions from aqueous solutions using local raw material as adsorbent: a study in binary systems, (2017),. <https://doi.org/10.5004/dwt.2017.20728>.
- [16] Luo, P., Zhao, Y., Zhang, B., Liu, J., Yang, Y., Liu, J., Study on the adsorption of Neutral Red from aqueous solution onto halloysite nanotubes, *Water Research*, 44 (5) (2010), 1489–1497. <https://doi.org/10.1016/j.watres.2009.10.042>.

- [17] Kuila, U., Prasad, M., Specific surface area and pore-size distribution in clays and shales, *Geophysical Prospecting*, 61 (2013), 341–362. <https://doi.org/10.1111/1365-2478.12028>.
- [18] Taylor, R.K., Cation Exchange in Clays And Mudrocks By Methylene Blue, *Journal of Chemical Technology and Biotechnology. Chemical Technology*, 35 (4) (1985), 195–207. <https://doi.org/10.1002/jctb.5040350407>.
- [19] El-Hinnawi, E., Abayazeed, S.D., El-Hinnawi, E., Characterization of Egyptian Smectitic Clay Deposits by Methylene Blue Adsorption, *American Journal of Applied Sciences*, 8 (12) (2011), 1282–1286.
- [20] Duc, M., Gaboriaud, F., Thomas, F., Sensitivity of the acid-base properties of clays to the methods of preparation and measurement: 2. Evidence from continuous potentiometric titrations, *Journal of Colloid and Interface Science*, 289 (1) (2005), 148–156. <https://doi.org/10.1016/j.jcis.2005.03.057>.
- [21] Ertaş, M., Acemioğlu, B., Alma, M.H., Usta, M., Removal of methylene blue from aqueous solution using cotton stalk, cotton waste and cotton dust, *Journal of Hazardous Materials*, 183 (1–3) (2010), 421–427. <https://doi.org/10.1016/j.jhazmat.2010.07.041>.
- [22] Foo, K.Y., Hameed, B.H., Insights into the modeling of adsorption isotherm systems, *Chemical Engineering Journal*, 156 (2010), 2–10. <https://doi.org/10.1016/j.cej.2009.09.013>.
- [23] Salarirad, M.M., Behnamfard, A., Modeling of equilibrium data for free cyanide adsorption onto activated carbon by linear and non-linear regression methods, *International Conference on Environment and Industrial Innovation*, 12 (2011), 79–84.
- [24] Rahman, M.S., Sathasivam, K. V., Heavy metal adsorption onto kappaphycus sp. from aqueous solutions: The use of error functions for validation of isotherm and kinetics models, *BioMed Research International*, 2015 (2015), <https://doi.org/10.1155/2015/126298>.
- [25] Samarghandi, M., Hadi, M., Moayedi, S., Askari, F.B., Adsorption of Heavy Metals from Waste Streams By Peat., *Journal of Environmental Health Science & Engineering*, 6 (4) (2009), 285–294. <https://ijehse.tums.ac.ir/index.php/jehse/article/view/223> (accessed May 30, 2021).
- [26] Wong, Y.C., Szeto, Y.S., Cheung, W.H., McKay, G., Equilibrium studies for acid dye adsorption onto chitosan, *Langmuir*, 19 (19) (2003), 7888–7894. <https://doi.org/10.1021/la030064y>.
- [27] Dada, A.O., Olalekan, A.P., Olatunya, A.M., Dada, O., Langmuir, Freundlich, Temkin and Dubinin–Radushkevich isotherms studies of equilibrium sorption of Zn<sup>2+</sup> unto phosphoric acid modified rice husk, *IOSR Journal of Applied Chemistry*, 3 (1) (2012), 38–45.
- [28] Yuh-Shan, H., Adsorption of Heavy Metals from Waste Streams By Peat, The University of Birmingham, 1995.

- [29] El-Sikaily, A., Nemr, A. El, Khaled, A., Abdelwehab, O., Removal of toxic chromium from wastewater using green alga *Ulva lactuca* and its activated carbon, *Journal of Hazardous Materials*, 148 (1–2) (2007), 216–228. <https://doi.org/10.1016/j.jhazmat.2007.01.146>.
- [30] Lagergren, S., Zur theorie der sogenannten adsorption gelöster stoffe, *K. Vet. Akad. Handl*, 24 (1898), 1–39.
- [31] Al-Musawi, T.J., Brouers, F., Zarrabi, M., Kinetic modeling of antibiotic adsorption onto different nanomaterials using the Brouers–Sotolongo fractal equation, *Environmental Science and Pollution Research*, 24 (4) (2017), 4048–4057. <https://doi.org/10.1007/s11356-016-8182-z>.
- [32] Gutzow, I., Todorova, S., Jordanov, N., Kinetics of chemical reactions and phase transitions at changing temperature: General reconsiderations and a new approach, (2010), 79–102.
- [33] Gökırmak, E.S., Karataş, Y., Gülcan, M., Kılıç, N.Ç., Enhancement of adsorption capacity of reduced graphene oxide by sulfonic acid functionalization: Malachite green and Zn (II) uptake, *Materials Chemistry and Physics*, 256 (2020), 123662. <https://doi.org/10.1016/j.matchemphys.2020.123662>.
- [34] Vilvanathan, S., Shanthakumar, S., Ni<sup>2+</sup> and Co<sup>2+</sup> adsorption using *Tectona grandis* biochar: kinetics, equilibrium and desorption studies, *Environmental Technology (United Kingdom)*, 39 (4) (2018), 464–478. <https://doi.org/10.1080/09593330.2017.1304454>.
- [35] Robati, D., Pseudo-second-order kinetic equations for modeling adsorption systems for removal of lead ions using multi-walled carbon nanotube, *Journal of Nanostructure in Chemistry*, 3 (1) (2013), 1–6.
- [36] Aksu, Z., Determination of the equilibrium, kinetic and thermodynamic parameters of the batch biosorption of nickel(II) ions onto *Chlorella vulgaris*, *Process Biochemistry*, 38 (1) (2002), 89–99. [https://doi.org/10.1016/S0032-9592\(02\)00051-1](https://doi.org/10.1016/S0032-9592(02)00051-1).
- [37] Li, Y.S., Liu, C.C., Chiou, C.S., Adsorption of Cr(III) from wastewater by wine processing waste sludge, *Journal of Colloid and Interface Science*, 273 (1) (2004), 95–101. <https://doi.org/10.1016/j.jcis.2003.12.051>.
- [38] Mohellebi, F., Lakel, F., Adsorption of Zn<sup>2+</sup> on Algerian untreated bentonite clay, *Desalination and Water Treatment*, 57 (13) (2016), 6051–6062. <https://doi.org/10.1080/19443994.2015.1006255>.
- [39] Sarıkaya, Y., Önal, M., An indirect model for sintering thermodynamics, *Turkish Journal of Chemistry*, 40 (2016), 841 – 845. <https://doi.org/10.3906/kim-1603-61>.
- [40] Errais, E., Duplay, J., Darragi, F., M'Rabet, I., Aubert, A., Huber, F., Morvan, G., Efficient anionic dye adsorption on natural untreated clay: Kinetic study and thermodynamic parameters, *Desalination*, 275 (1–3) (2011), 74–81. <https://doi.org/10.1016/j.desal.2011.02.031>.

- [41] Rozalén, M., Brady, P. V., Huertas, F.J., Surface chemistry of K-montmorillonite: Ionic strength, temperature dependence and dissolution kinetics, *Journal of Colloid and Interface Science*, 333 (2) (2009), 474–484. <https://doi.org/10.1016/j.jcis.2009.01.059>.
- [42] Worch, E., Adsorption Technology in Water Treatment, in: Adsorption Technology in Water Treatment, De Gruyter, Germany, 2012: pp. 1–345. <https://doi.org/10.1515/9783110240238>.
- [43] Belhouchat, N., Zaghouane-Boudiaf, H., Viseras, C., Removal of anionic and cationic dyes from aqueous solution with activated organo-bentonite/sodium alginate encapsulated beads, *Applied Clay Science*, 135 (2017), 9–15. <https://doi.org/10.1016/j.clay.2016.08.031>.
- [44] Caliskan, N., Kul, A.R., Alkan, S., Sogut, E.G., Alacabey, I., Adsorption of Zinc(II) on diatomite and manganese-oxide-modified diatomite: A kinetic and equilibrium study, *Journal of Hazardous Materials*, 193 (2011), 27–36. <https://doi.org/10.1016/j.jhazmat.2011.06.058>.
- [45] Miraboutalebi, S.M., Nikouzad, S.K., Peydayesh, M., Allahgholi, N., Vafajoo, L., McKay, G., Methylene blue adsorption via maize silk powder: Kinetic, equilibrium, thermodynamic studies and residual error analysis, *Process Safety and Environmental Protection*, 106 (2017), 191–202. <https://doi.org/10.1016/j.psep.2017.01.010>.
- [46] Sdiri, A., Khairy, M., Bouaziz, S., El-Safty, S., A natural clayey adsorbent for selective removal of lead from aqueous solutions, *Applied Clay Science*, 126 (2016), 89–97. <https://doi.org/10.1016/j.clay.2016.03.003>.
- [47] Smidt, E., Meissl, K., The applicability of Fourier transform infrared (FT-IR) spectroscopy in waste management, *Waste Management*, 27 (2) (2007), 268–276. <https://doi.org/10.1016/j.wasman.2006.01.016>.
- [48] Zou, W., Bai, H., Gao, S., Competitive adsorption of neutral red and Cu<sup>2+</sup> onto pyrolytic char: Isotherm and kinetic study, *Journal of Chemical and Engineering Data*, 57 (10) (2012), 2792–2801. <https://doi.org/10.1021/je300686u>.
- [49] Pavan, F.A., Lima, E.C., Dias, S.L.P., Mazzocato, A.C., Methylene blue biosorption from aqueous solutions by yellow passion fruit waste, *Journal of Hazardous Materials*, 150 (3) (2008), 703–712. <https://doi.org/10.1016/j.jhazmat.2007.05.023>.
- [50] Ferrage, E., Lanson, B., Sakharov, B.A., Drits, V.A., Investigation of smectite hydration properties by modeling experimental X-ray diffraction patterns: Part I: Montmorillonite hydration properties, *American Mineralogist*, 90 (8–9) (2005), 1358–1374. <https://doi.org/10.2138/am.2005.1776>.
- [51] Garcia-Valles, M., Alfonso, P., Martínez, S., Roca, N., Mineralogical and thermal characterization of kaolinitic clays from terra alta (Catalonia,

- Spain), *Minerals*, 10 (2) (2020), <https://doi.org/10.3390/min10020142>.
- [52] Arfaoui, S., Frini-Srasra, N., Srasra, E., Modelling of the adsorption of the chromium ion by modified clays, *Desalination*, 222 (1–3) (2008), 474–481. <https://doi.org/10.1016/j.desal.2007.03.014>.
- [53] Adeniyi, F.I., Ogundiran, M.B., Hemalatha, T., Hanumantrai, B.B., Characterization of raw and thermally treated Nigerian kaolinite-containing clays using instrumental techniques, *SN Applied Sciences* 2020 2:5, 2 (5) (2020), 1–14. <https://doi.org/10.1007/S42452-020-2610-X>.
- [54] Thao, H.-M., Characterization of Clays and Clay Minerals for Industrial Applications: Substitution non-Natural Additives by Clays in UV Protection, Ernst-Moritz-Arndt-University Greifswald, 2006.
- [55] Sdiri, A., Higashi, T., Hatta, T., Jamoussi, F., Tase, N., Evaluating the adsorptive capacity of montmorillonitic and calcareous clays on the removal of several heavy metals in aqueous systems, *Chemical Engineering Journal*, 172 (1) (2011), 37–46. <https://doi.org/10.1016/j.cej.2011.05.015>.
- [56] Laus, R., De Fávère, V.T., Competitive adsorption of Cu(II) and Cd(II) ions by chitosan crosslinked with epichlorohydrin-triphosphate, *Bioresource Technology*, 102 (19) (2011), 8769–8776. <https://doi.org/10.1016/j.biortech.2011.07.057>.
- [57] Tan, I.A.W., Ahmad, A.L., Hameed, B.H., Adsorption of basic dye on high-surface-area activated carbon prepared from coconut husk: Equilibrium, kinetic and thermodynamic studies, *Journal of Hazardous Materials*, 154 (1–3) (2008), 337–346. <https://doi.org/10.1016/j.jhazmat.2007.10.031>.
- [58] Gökırmak, S.E., Çalışkan, K.N., Isotherm and Kinetic Studies of Pb(II) Adsorption on Raw And Modified Diatomite By Using Non-Linear Regression Method, *FRESENIUS ENVIRONMENTAL BULLETIN*, 26 (4) (2017), 2720–2728.
- [59] Kumar, K.V., Porkodi, K., Rocha, F., Comparison of various error functions in predicting the optimum isotherm by linear and non-linear regression analysis for the sorption of basic red 9 by activated carbon, *Journal of Hazardous Materials*, 150 (1) (2008), 158–165. <https://doi.org/10.1016/j.jhazmat.2007.09.020>.
- [60] Al-Ghouti, M.A., Da'ana, D.A., Guidelines for the use and interpretation of adsorption isotherm models: A review, *Journal of Hazardous Materials*, 393 (2020), 122383. <https://doi.org/10.1016/j.jhazmat.2020.122383>.
- [61] Revellame, E.D., Fortela, D.L., Sharp, W., Hernandez, R., Zappi, M.E., Adsorption kinetic modeling using pseudo-first order and pseudo-second order rate laws: A review, *Cleaner Engineering and Technology*, 1 (2020), 100032. <https://doi.org/10.1016/j.clet.2020.100032>.
- [62] Plazinski, W., Dziuba, J., Rudzinski, W., Modeling of sorption kinetics: The pseudo-second order equation and the sorbate intraparticle diffusivity,

- Adsorption*, 19 (5) (2013), 1055–1064. <https://doi.org/10.1007/s10450-013-9529-0>.
- [63] Ahmad, M.A., Ahmad Puad, N.A., Bello, O.S., Kinetic, equilibrium and thermodynamic studies of synthetic dye removal using pomegranate peel activated carbon prepared by microwave-induced KOH activation, *Water Resources and Industry*, 6 (2014), 18–35. <https://doi.org/10.1016/j.wri.2014.06.002>.
- [64] Inyinbor, A.A., Adekola, F.A., Olatunji, G.A., Kinetics, isotherms and thermodynamic modeling of liquid phase adsorption of Rhodamine B dye onto *Raphia hookerie* fruit epicarp, *Water Resources and Industry*, 15 (2016), 14–27. <https://doi.org/10.1016/j.wri.2016.06.001>.
- [65] Al-Ghouti, M.A., Al-Absi, R.S., Mechanistic understanding of the adsorption and thermodynamic aspects of cationic methylene blue dye onto cellulosic olive stones biomass from wastewater, *Scientific Reports*, 10 (1) (2020), 1–18. <https://doi.org/10.1038/s41598-020-72996-3>.
- [66] Haro, N.K., Dávila, I.V.J., Nunes, K.G.P., de Franco, M.A.E., Marcilio, N.R., Féris, L.A., Kinetic, equilibrium and thermodynamic studies of the adsorption of paracetamol in activated carbon in batch model and fixed-bed column, *Applied Water Science*, 11 (2) (2021), 38. <https://doi.org/10.1007/s13201-020-01346-5>.
- [67] Saha, P., Chowdhury, S., Insight Into Adsorption Thermodynamics, *Thermodynamics*, (2011),. <https://doi.org/10.5772/13474>.
- [68] Boukhemkhem, A., Rida, K., Improvement adsorption capacity of methylene blue onto modified Tamazert kaolin, *Adsorption Science & Technology*, 35 (9) (2017), 2017. <https://doi.org/10.1177/0263617416684835>.
- [69] Banerjee, S., Chattopadhyaya, M.C., Adsorption characteristics for the removal of a toxic dye, tartrazine from aqueous solutions by a low cost agricultural by-product, *Arabian Journal of Chemistry*, 10 (2017), S1629–S1638. <https://doi.org/10.1016/j.arabjc.2013.06.005>.